Journal of Sound and Vibration (2000) **229**(4), 973–991
doi:10.1006/jsvi.1999.2518, available online at http://www.idealibrary.com on IDEAL®

MODE IDENTIFICATION OF HIGH-AMPLITUDE PRESSURE WAVES IN LIQUID ROCKET ENGINES

R. Ebrahimi, K. Mazaheri and A. Ghafourian

Sharif University of Technology, Mechanical Engineering Department, Tehran 11365-9567, *Iran*

(*Received* 30 *November* 1998, *and in final form* 28 *July* 1999)

Identification of existing instability modes from experimental pressure measurements of rocket engines is difficult, specially when steep waves are present. Actual pressure waves are often non-linear and include steep shocks followed by gradual expansions. It is generally believed that interaction of these non-linear waves is difficult to analyze. A method of mode identification is introduced. After presumption of constituent modes, they are superposed by using a standard finite difference scheme for solution of the classical wave equation. Waves are numerically produced at each end of the combustion tube with different wavelengths, amplitudes, and phases with respect to each other. Pressure amplitude histories and phase diagrams along the tube are computed. To determine the validity of the presented method for steep non-linear waves, the Euler equations are numerically solved for non-linear waves, and negligible interactions between these waves are observed. To show the applicability of this method, other's experimental results in which modes were identified are used. Results indicate that this simple method can be used in analyzing complicated pressure signal measurements.

1. INTRODUCTION

To obtain an effective procedure for the design of liquid-propellant rocket engines, the control of the combustion process is necessary. Combustion instability remains one of the most critical problems in the development of liquid-propellant rocket engines. This phenomenon consists of a forced oscillation of combustion gases driven by the combustion process interacting with the resonance effects of the chamber geometry [1–3].

Oscillatory operation of a rocket engine is undesirable for many reasons. One of the most important of these is severe vibration (greater than 1000 g). Such vibration levels can impair the operation of sensitive guidance components. Another severe effect is the grossly increased heat transfer due to the oscillatory operation. This increase is often sufficient to melt and destroy portions of the rocket system in a fraction of a second [3, 4].

Combustion instabilities may be regarded as the unsteady motion of a dynamic system capable of sustaining oscillations over a broad range of frequencies [5]. If

0022-460X/00/040973 + 19 $35.00/0

the amplitude is small, the instability is closely related to classical acoustic behavior occurring in the absence of combustion and mean flow. The geometry of the chamber is therefore a dominant influence. Corresponding to classical results, travelling and standing waves are found [2, 5, 6]. They are driven by the combustion process energy released influenced by the mean flow as well as by the conditions at the injector face and exhaust.

Under suitable circumstances the flow of energy to the waves may dominate the losses in such a way that non-linear behavior becomes significant. In extreme cases, shock waves may be formed. The propagation speed of disturbances is a weak function of the amplitude, thus, the frequencies do not differ greatly from classical values computed for the same geometry.

There are three recognized types of the combustion instability. The first type is the low-frequency instability (10–200 Hz), which is due to interactions between the processes taking place in the combustion chamber and the propellant feed system. The intermediate-frequency instability (200–1000 Hz) is the second type. It results from a so-called entropy wave produced cyclically in the chamber and interacting with the exhaust nozzle. Intermediate-frequency instability is the least frequently observed type. The third type is the high-frequency instability (greater than 1000 Hz), which consists of excitation of acoustic vibrational modes of the combustion chamber. This is by far the most destructive kind of instability and hardest to control [6, 7].

In an actual engine with high-frequency instability several modes could be present simultaneously. These modes may correspond to the longitudinal, radial or tangential modes of the chamber. They could be of travelling or standing nature. Pressure signal measurements from the chamber have been used to determine the modes [3, 8, 9]. Fast Fourier transform of pressure signals, which is commonly used for this purpose, is not sufficient when standing steep waves are present. As will be shown in section 4.2, it may overestimate the frequency of these instability modes. Using high-speed photography and film recording, luminosity from a two-dimensional transparent-wall combustion chamber has also been used to determine the instability modes [3, 10, 11].

A simple linear method applicable for analysis of experimental measurements done for detection of combustion instability mode is presented. In this method, by reconstruction of measured pressure waves and their phase variation along the chamber, the instability modes can be identified. For this purpose, by presumption of the instability modes, the appropriate waves are produced numerically at each end of a combustion tube with appropriate amplitude and frequency. With these boundary conditions the classical acoustic equations are solved. Experimentally produced amplitude and phase time histories are examined and compared against their presumed theoretical equivalents to identify the instability modes present.

For reconstruction of non-linear steep waves, the validity of this linear method must be verified. By numerical solution of the non-linear Euler equation, propagation and interaction of steep waves are studied. Results indicate that the non-linearity of waves has negligible influence on their mechanism of interaction. Thus, one may superpose the non-linear waves for this particular application.

In the following sections, numerical solution of the linear waves, validity of the superposition assumption for non-linear steep waves and the application of the present method in mode identification, are described.

2. NUMERICAL SOLUTION OF THE LINEAR WAVES

To arrive at the classical wave equation, the mass, momentum, and energy equations are linearized for an inviscid, adiabatic, non-reactive, and quiescent media. The following equation is obtained:

$$\nabla^2 p = \frac{1}{a^2}\frac{\partial^2 p}{\partial t^2} \tag{1}$$

in which a is the speed of sound. This equation is written as a system of first order equations

$$\frac{\partial p}{\partial t} = \pm a\frac{\partial p}{\partial x}, \tag{2}$$

where + and − signs pertain to right- and left-travelling waves. For discretization of these equations, the first order upwind scheme is used:

$$\frac{p_i^{n+1} - p_i^n}{\Delta t} = -\frac{a}{\Delta x}(p_i^n - p_{i-1}^n) \quad \text{(RTW)}. \tag{3}$$

For left-travelling waves (LTW) a similar equation can be written. In the particular case $c = a\Delta t/\Delta x = 1$, the numerical solution is the same as the exact solution of the wave equation.

Specific modes are generated in a combustion tube with both ends open. A left travelling wave with particular amplitude is generated continuously at the right end. The left end of the tube is assumed to act as an open end with respect to this left-travelling wave. At the same time a right-travelling wave is continuously generated at the left end for which the right end is assumed to be open. Depending on the mode which is to be generated, different amplitude and phase can be assigned to each of these imposed waves.

With these boundary conditions, equation (2) is solved by the above-mentioned scheme. Pressure and phase history are computed along the tube for that particular mode. Application of this method for interaction of non-linear waves is questionable. This is the subject of the following section.

3. SUPERPOSITION OF THE NON-LINEAR WAVES

In the combustion chamber of rockets, the chemical reaction of propellants gives high energy density to the compressible gases within the chamber. Combustion

processes can couple with unsteady motion of gases. The flow of a small portion of the total combustion energy to the acoustic waves may dominate the losses such that non-linear behavior becomes significant and shock waves may form. Under these conditions, the validity of results from the classical wave equation has to be determined. It must be shown that while the formation of steep waves are non-linear, their propagation and interaction are approximately linear.

The propagation and interaction of non-linear steep waves are studied by numerical solution of the non-linear Euler equation. The variation of amplitude and area of a wave during interaction and collision with another wave are two parameters which are used to determine the influence of non-linear effects on the wave deformation. These parameters are computed for a wave during its propagation, and are compared with parameters which are found for the same wave without any collision. If the difference of these parameters in the two cases are negligible, we may assume that the superposition of non-linear waves is valid for this particular application.

3.1. NUMERICAL SOLUTION OF THE NON-LINEAR WAVES

To prove the above hypothesis, propagation and collision of non-linear waves in a one-dimensional tube is studied by solving the Euler equations. The governing equations is

$$\frac{\partial \mathbf{U}}{\partial t} + \frac{\partial \mathbf{F}}{\partial x} = 0, \tag{4}$$

where two vectors $\mathbf{U}$ and $\mathbf{F}$ are

$$\mathbf{U} = \begin{pmatrix} \rho \\ \rho u \\ \rho E \end{pmatrix}, \qquad \mathbf{F} = \begin{pmatrix} \rho u \\ \rho u^2 + p \\ \rho u H \end{pmatrix} \tag{5}$$

in which u, E, and H are the velocity, total internal energy, and total enthalpy respectively. For discretization on a numerical grid, equation (4) is integrated over the ith cell, to find

$$\frac{\partial \mathbf{U}_i}{\partial t} = -\frac{1}{\Delta v_i} \sum_{sides} (\tilde{\mathbf{F}} \cdot S), \tag{6}$$

where S and v are the cell face area and volume respectively. According to the van Leer flux vector splitting [12], the flux vectors become

$$F_1^{\pm} = \pm \tfrac{1}{4} \rho a (M \pm 1)^2, \tag{7}$$

$$F_2^{\pm} = F_1^{\pm}\left(u - \frac{p}{\rho a^2}(u \mp 2a)\right), \tag{8}$$

$$F_3^{\pm} = F_1^{\pm}\left(H - \frac{h/a^2}{1 + 2h/a^2}(u \mp a)^2\right) \tag{9}$$

in which h is the enthalpy and M is the Mach number.

The monotone upstream-centered schemes for conservation laws (MUSCL) method is used to increase the spatial order of accuracy [13]. In this method, primitive variables are defined as follows:

$$\tilde{\mathbf{U}}^t = (\rho, u, p). \tag{10}$$

The numerical flux vector in $i + \frac{1}{2}$ side is written as

$$\tilde{\mathbf{F}}_{i+1/2} = \mathbf{F}^+(\tilde{\mathbf{U}}^L_{i+1/2}) + \mathbf{F}^-(\tilde{\mathbf{U}}^R_{i+1/2}). \tag{11}$$

General forms of the primitive variable vectors $\tilde{\mathbf{U}}^R_{i+1/2}$ and $\tilde{\mathbf{U}}^L_{i+1/2}$, when including the Minmod flux limiter functions, are

$$\tilde{\mathbf{U}}^L_{i+1/2} = \tilde{\mathbf{U}}_i + \frac{\theta}{4}((1-\kappa)\boldsymbol{\phi}^- + (1+\kappa)\boldsymbol{\phi}^+)_i, \tag{12}$$

$$\tilde{\mathbf{U}}^R_{i+1/2} = \tilde{\mathbf{U}}_{i+1} - \frac{\theta}{4}((1-\kappa)\boldsymbol{\phi}^+ + (1+\kappa)\boldsymbol{\phi}^-)_{i+1}. \tag{13}$$

For $\theta = 1$ and $\kappa = \frac{1}{3}$, the third order upwind is achieved. More information on this method and the functions $\boldsymbol{\phi}^-$ and $\boldsymbol{\phi}^+$ is reported by Yee [14].

3.2. THE SUPERPOSITION HYPOTHESIS OF NON-LINEAR WAVES

The coupling and mutual effects of a high-amplitude right- and left-travelling wave are studied by solving the non-linear Euler equations. The superposition hypothesis of non-linear waves is confirmed, if interaction of the waves does not change their shape and amplitude after they have passed over each other.

Consider a one-dimensional pipe with both ends open and an initial pressure distribution of

$$p = p_0 + \begin{cases} p_- \sin[\frac{2\pi}{\lambda}(x - x_R)], & x_R \leqslant x \leqslant x_R + \frac{\lambda}{2}, \\ p_+ \sin[\frac{2\pi}{\lambda}(x - x_L)], & x_L \leqslant x \leqslant x_L + \frac{\lambda}{2}, \\ 0 & \text{elsewhere}, \end{cases} \tag{14}$$

where λ is the wavelength. This initial pressure distribution includes two half sine waves at points x_R and x_L. The coefficients p_+ and p_- represent the amplitude of

the right- and left-travelling waves, respectively, and p_0 is the reference pressure. It is assumed that $p_+ = p_- = \tilde{p}$. In order to study the collision of these two waves, initial conditions of the other properties are calculated from Riemann invariants such that the waves positioned at x_R and x_L travel to left and right respectively. Thus, initial conditions of the other properties are [15]

$$\frac{u}{a_0} = \pm \frac{2}{\gamma - 1}\left[\left(\frac{p}{p_0}\right)^{(\gamma-1)/2\gamma} - 1\right], \tag{15}$$

$$\frac{T}{T_0} = \left[1 \pm \frac{\gamma - 1}{2}\left(\frac{u}{a_0}\right)\right]^2, \tag{16}$$

where + and − indicate the properties of the right- and left-travelling waves respectively. Neumann boundary condition is assumed on both sides of the pipe. For small values of $\tilde{p}$, the shape of these waves does not change during travelling and collision. By increasing the value of $\tilde{p}$, the wavefront speed increases such that the waves quickly transform into shock and expansion waves, as shown in Figure 1(a). For this condition, when the left-travelling wave has passed the other wave and positioned at a particular location, its amplitude and area under the curve are computed. Also, in the absence of the right-travelling wave, the same values are calculated by the same method for the left-travelling wave when it is at the same position.

The ratios of amplitude change $\delta p/p^*$ and area under the curve change $\delta A/A^*$ for the left-travelling wave at the particular position for two different conditions mentioned above are determined. In these ratios p^* and A^* represent the amplitude and area under the curve of the travelling wave just before collision with another wave. Since the distances travelled by the wave in both cases are the same, it is expected that the dissipation and dispersion of the numerical method is almost cancelled out of the mentioned ratios. The computation is done for different values of p^*/p_0. Figure 1(b) shows the behavior of the $\delta p/p^*$ and $\delta A/A^*$ with respect to p^*/p_0. As seen, even when the amplitude of the sharp wave is 2·2 times the reference pressure, the ratios of amplitude change is only 1·6% and ratio of area change is 0·85%. Therefore, the superposition hypothesis of non-linear waves holds with good accuracy for conditions of $p^*/p_0 < 2$. In experimental observations of liquid rocket engine instabilities done so far, the ratio p^*/p_0 is less than 1·75 [16]. Thus, it is concluded that classical acoustic theory can be used in the analysis of the waves coupling in the liquid rocket engines.

3.3. ANALYTICAL METHOD FOR SUPERPOSITION OF NON-LINEAR WAVES

According to the results of the previous section, the pressure field for a given non-linear wave can be predicted theoretically. This method is useful for conditions where an analytical solution is needed and also for determination of acoustic modes present in non-linear instabilities in an engine.

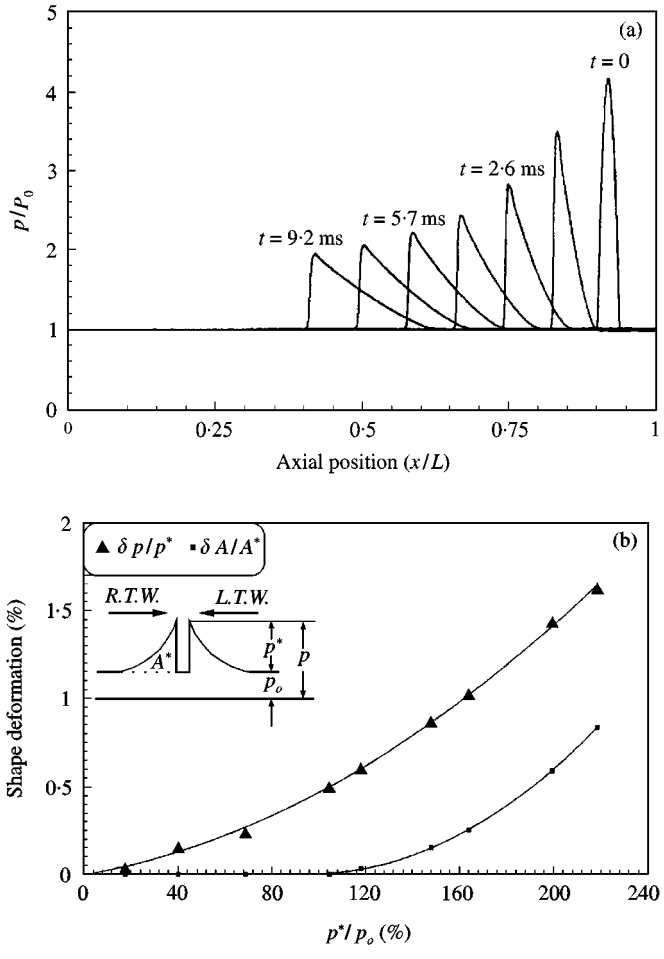

Figure 1. Non-linear wave propagation. (a) Sequence of conversion of a sine wave to a steep wave. (b) Shape deformation of a non-linear wave due to interaction with another non-linear wave with respect to intensity of the wave.

To simulate a cycle of sudden increase of pressure followed by a gradual expansion, we use a cubic power function, periodically regenerated. Consider two series of right- and left-travelling waves f and g for $-\infty < x < +\infty$, initially as

$$f(x) = \left(\frac{x}{\lambda} - n\right)^3, \quad n \leqslant \frac{x}{\lambda} < n + 1, \tag{17}$$

$$g(x) = \left(n + 1 - \frac{x}{\lambda}\right)^3, \quad n \leqslant \frac{x}{\lambda} < n + 1, \tag{18}$$

where n is an integer parameter, varying between $-\infty$ and $+\infty$. For $x/\lambda = n$, f has its minimum and g has its maximum values. For $x/\lambda = n + 1$, f has its maximum and g has its minimum values. Combination of f and g in the range of $0 < x/L < 1$

represents the presence of sharp waves in a pipe with a length of L at $t = 0$. To determine the wave shape at later times, the waves represented by f and g must travel to the right and left, respectively, which gives

$$f(x, t) = \left(\frac{x - at}{\lambda} - n\right)^3, \quad n \leqslant \frac{x - at}{\lambda} < n + 1, \tag{19}$$

$$g(x, t) = \left(n + 1 - \frac{x + at}{\lambda}\right)^3, \quad n \leqslant \frac{x + at}{\lambda} < n + 1. \tag{20}$$

To generate the second mode, the wavelength must be equal to the length of the pipe, $\lambda = L$. The other modes can similarly be generated by choosing appropriate wavelength and phase differences for the f and g waves. To generate the odd modes in a pipe with both ends closed, unlike the even modes which do not need a phase difference between f and g waves, a value of $\lambda/2$ must be subtracted from the x variable of the g wave. For example to generate the third mode, the wavelength must be $(2L/3)$ and $(1/2)(2L/3)$ must be subtracted from the x variable of the g wave. This analytic solution may be used in analysis of combinations of non-linear instabilities in engines. For example if some dominant non-linear unstable modes is guessed, pressure evaluation should be compared with the corresponding analytic solution, to see if the guess is right. If more one mode is present, it is hard to analyze measured data.

4. APPLICATIONS IN ACTUAL SITUATIONS

To study different longitudinal modes in a pipe by the method of superposition of waves, at each end of a pipe a periodic wave with particular amplitude and frequency is generated numerically. From the right end, left-travelling waves and from the left end, right-travelling wave are imposed.

4.1. LINEAR WAVES

For generating the first longitudinal mode, harmonic waves with the same amplitude, a wave-length twice the pipe length and a phase difference of π radian is imposed on both ends of the pipe. The right- and left-travelling waves have the following form:

$$p\left(t, \frac{x}{L} = 0\right) = f_L(t) = p_+ \cos\left(\frac{\pi t}{\tau} + \pi\right) \quad \text{(RTW)}, \tag{21}$$

$$p\left(t, \frac{x}{L} = 1\right) = f_R(t) = p_- \cos\left(\frac{\pi t}{\tau}\right) \quad \text{(LTW)}, \tag{22}$$

where p_+, p_- and τ are the amplitude of right- and left-travelling waves and period of oscillation respectively. The curves representing the amplitude and phase angle

variation with respect to x/L are shown in Figure 2(a) and (b). Two regions can be identified in these figures. One region is where $0 < x/L < 0{\cdot}5$ and the other is in $0{\cdot}5 < x/L < 1$. Pressure reaches its limit at the same time for all points in these regions. Pressures in these two regions are 180° out of phase with respect to each other. Thus, the curve representing the phase angle is a step function and can be continued to infinity.

To generate the second longitudinal mode, harmonic waves with the same amplitude and a wavelength equal to the length of the pipe are imposed on both side of the pipe. The shapes of the right- and left-travelling waves are

$$p\left(t, \frac{x}{L} = 0\right) = f_L(t) = p_+ \cos\left(\frac{2\pi t}{\tau}\right) \quad \text{(RTW)}, \tag{23}$$

$$p\left(t, \frac{x}{L} = 1\right) = f_R(t) = p_- \cos\left(\frac{2\pi t}{\tau}\right) \quad \text{(LTW)}. \tag{24}$$

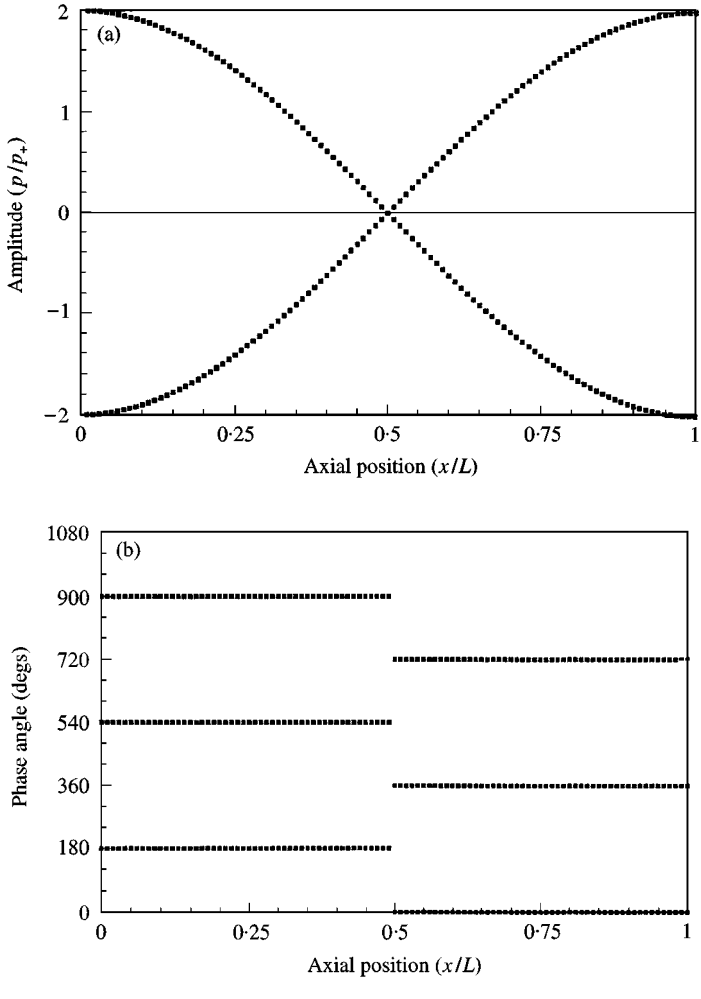

Figure 2. Envelope of amplitude and phase variation for first standing longitudinal wave in a pipe: (a) amplitude diagram; (b) phase diagram.

The curves indicating the amplitude and phase angle variation are shown in Figure 3(a) and (b). For $p_- = 0$, only a right-travelling wave exists in the pipe. The maximum and minimum pressures observed at different points in the pipe are constant equal to $\pm p_+$, as shown by curve $p_- = 0$ in Figure 3(a). Phase difference of pressure variation with respect to time at different points in the pipe changes linearly with x/L. Since the wavelength is the same as pipe length, the phase difference of pressure variation at the two ends is 360°, as shown by curve $p_- = 0$ in Figure 3(b). If $p_- = p_+$, the second standing mode exists in the pipe. For this case, two complete antinodes are observed in the envelope of amplitude variations. The time variation of pressure at all points between nodes and antinodes are in the same phase and are 180° out of phase with respect to the next node and antinode. In general, for the longitudinal standing modes there are the same number of nodes as the order of the mode. For $0 < p_- < p_+$, the envelope of amplitude and phase variations are between the above two extreme cases.

Right- and left-travelling waves with small frequency difference when entering the pipe were studied next. The wavelength of the right- and left-travelling waves are the same as the pipe length with a little difference to produce the desired frequency shift. Therefore, this precessing wave is the same as the second longitudinal mode, and two nodes exist in the pipe but their locations vary with time as in Figure 4(a). In this case, periodic pulsation is observed in the pressure variation with respect to time. From Figure 4(a) and (b), it can be observed that one node in the pipe at $t = 0$ is at $x/L = 0{\cdot}25$. This node moves to the left in time and reaches to the position $x/L = 0{\cdot}15$ at $t = 1$ ms as shown in Figure 4(a) and (c).

4.2. NON-LINEAR WAVES

The waves observed in the liquid-propellant rocket engines are mostly steep waves. The compression parts of the harmonic waves grow in amplitude due to non-linear effects as they propagate and become steep wave. To study this type of waves, two steep right- and left-travelling waves with amplitudes such as $p_+ = p_-$ and wavelength equal to the pipe length are generated at both ends of the pipe as in Figure 5(a). These waves are the sharpened form of the second longitudinal mode. Since at the moment of entrance of the wave from the right end, the wave propagating from the left exists in the same end, the amplitude becomes $2p_+$, and the same is true for the left-end wave.

From the solution of the classical acoustic equation with the above given boundary conditions, it is observed that unlike the standing second longitudinal mode where two nodes existed at locations $x/L = 0{\cdot}25$ and $0{\cdot}75$, no node is at these points for the steep waves. As shown in Figure 5(b), the time variation of pressure at these points indicates the presence of waves with a frequency twice that of entering waves and amplitude of p_+. From Figure 5(c) it can be seen that the time variation of pressure at the mid point of the pipe is the same as entering waves. At intervals $0 < x/L < 0{\cdot}25$, $0.25 < x/L < 0.75$ and $0{\cdot}75 < x/L < 1$, the time variation of pressure has two peaks. One peak corresponds to the right-travelling wave and the other to the left-travelling wave as in Figure 5(d) and (e). As we approach points

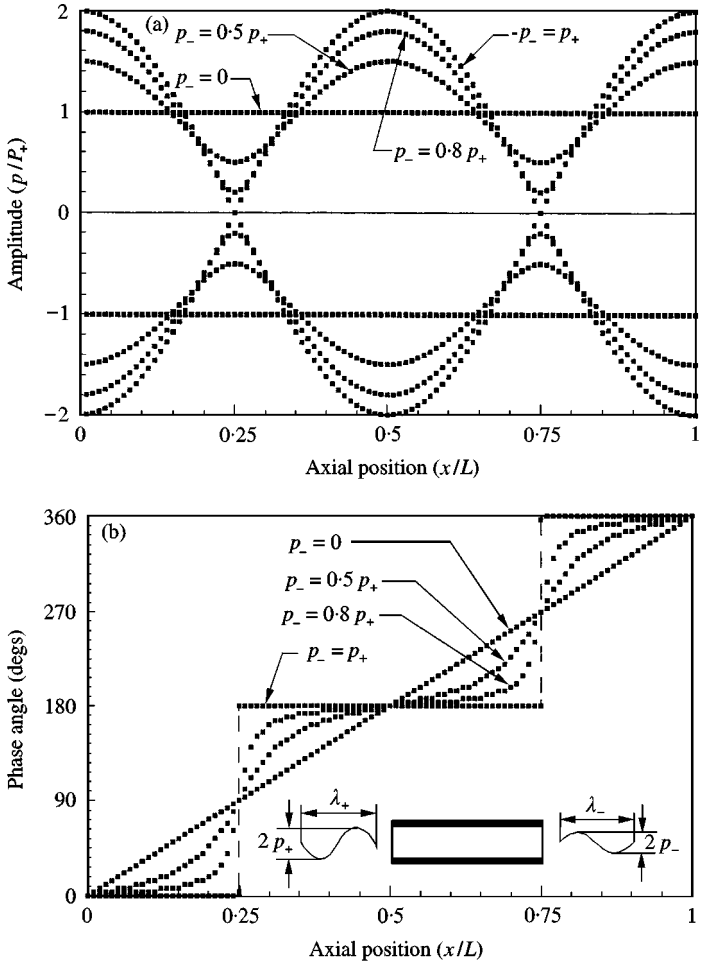

Figure 3. Envelope of amplitude and phase variation for opposed travelling waves in a pipe: (a) amplitude diagram; (b) phase diagram.

$x/L = 0{\cdot}25$ and $0{\cdot}75$, the distance of these peaks increases and finally their shapes become the same. The phase variation with respect to x/L is shown in Figure 5(f). Unlike the phase variation of second standing harmonic wave which has a stepwise shape, for the steepened case it has a diamond shape. Phase curve varies linearly with x/L. This curve is similar to the phase curve for consecutive impingement and reflection of longitudinal waves to the walls of a closed cavity.

A case in which at the same time several modes exist in the combustion chamber [3] is studied next. Such a condition can be observed during long operations of engines or during transition from one mode to another mode. Figure 6(a) shows the time variation of pressure at point $x/L = 0{\cdot}9$. The oscillations which are repeated continuously in this curve have eight peaks. Part (b) of Figure 6 shows the phase variation of pressure waves measured at different points of the engine. The dotted and continuous lines represent the first-travelling and third-standing modes

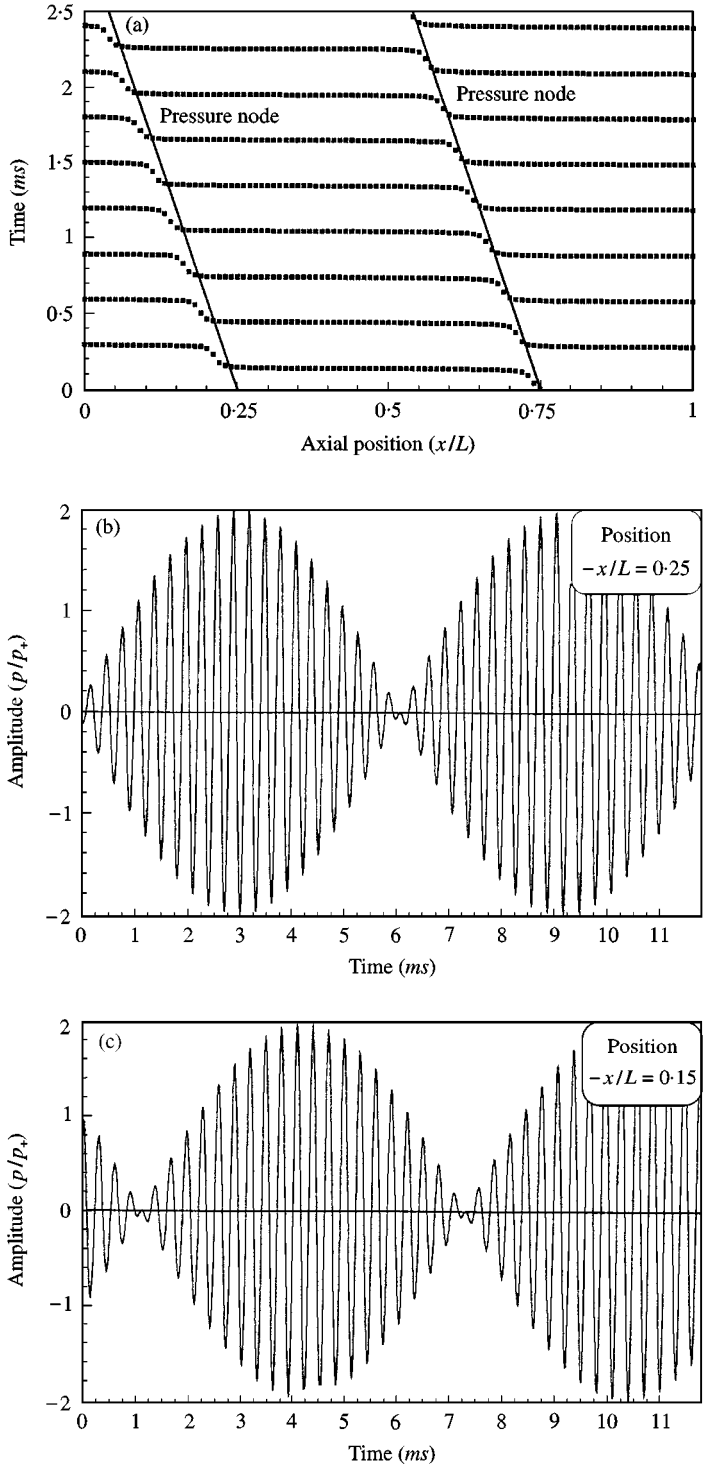

Figure 4. Precessing second longitudinal mode instability: (a) phase diagram; (b) time variation of pressure at $x/L = 0{\cdot}25$; (c) time variation of pressure at $x/L = 0{\cdot}05$.

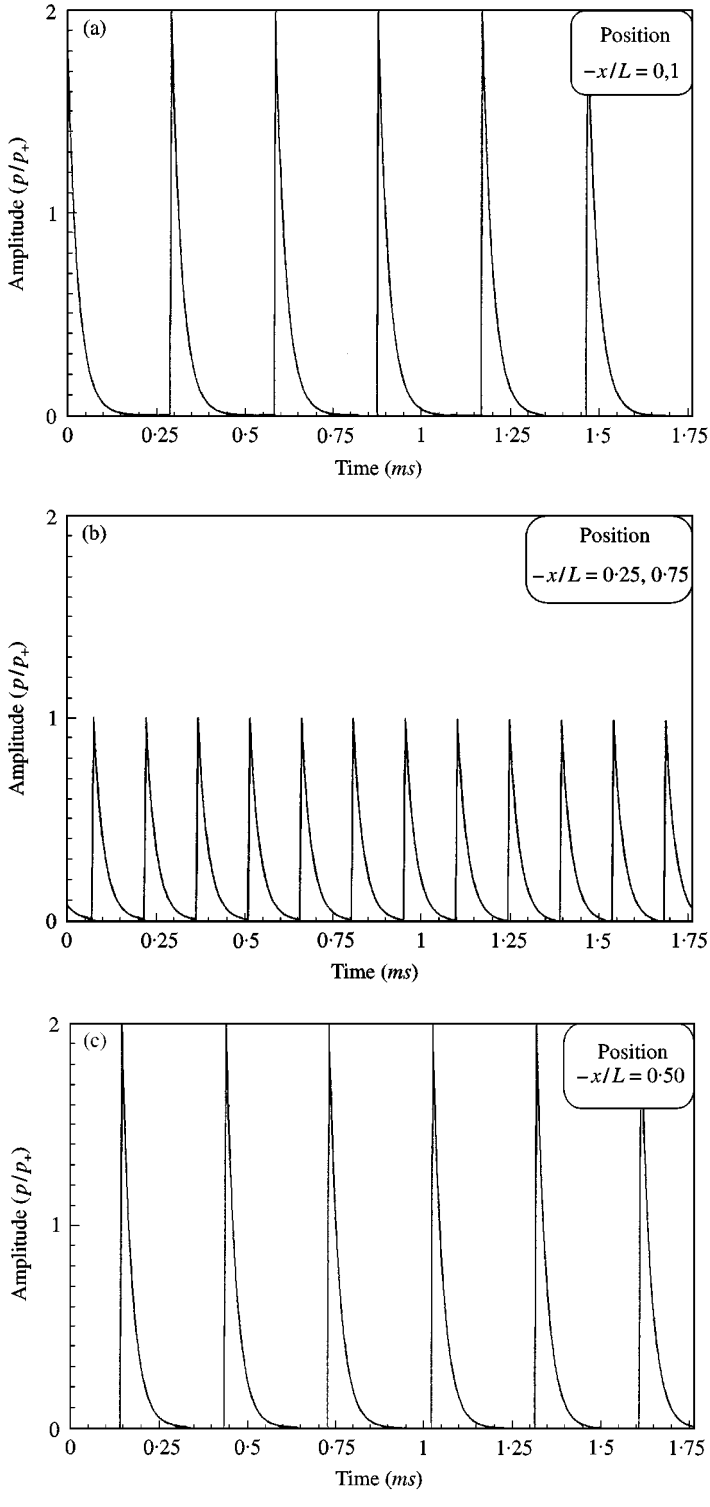

Figure 5. Time variation of pressure and phase diagrams for the second steep longitudinal wave in a pipe: (a) time variation of pressure at $x/L = 0{\cdot}1$; (b) time variation of pressure at $x/L = 0{\cdot}25$, $0{\cdot}75$; (c) time variation of pressure at $x/L = 0{\cdot}5$;

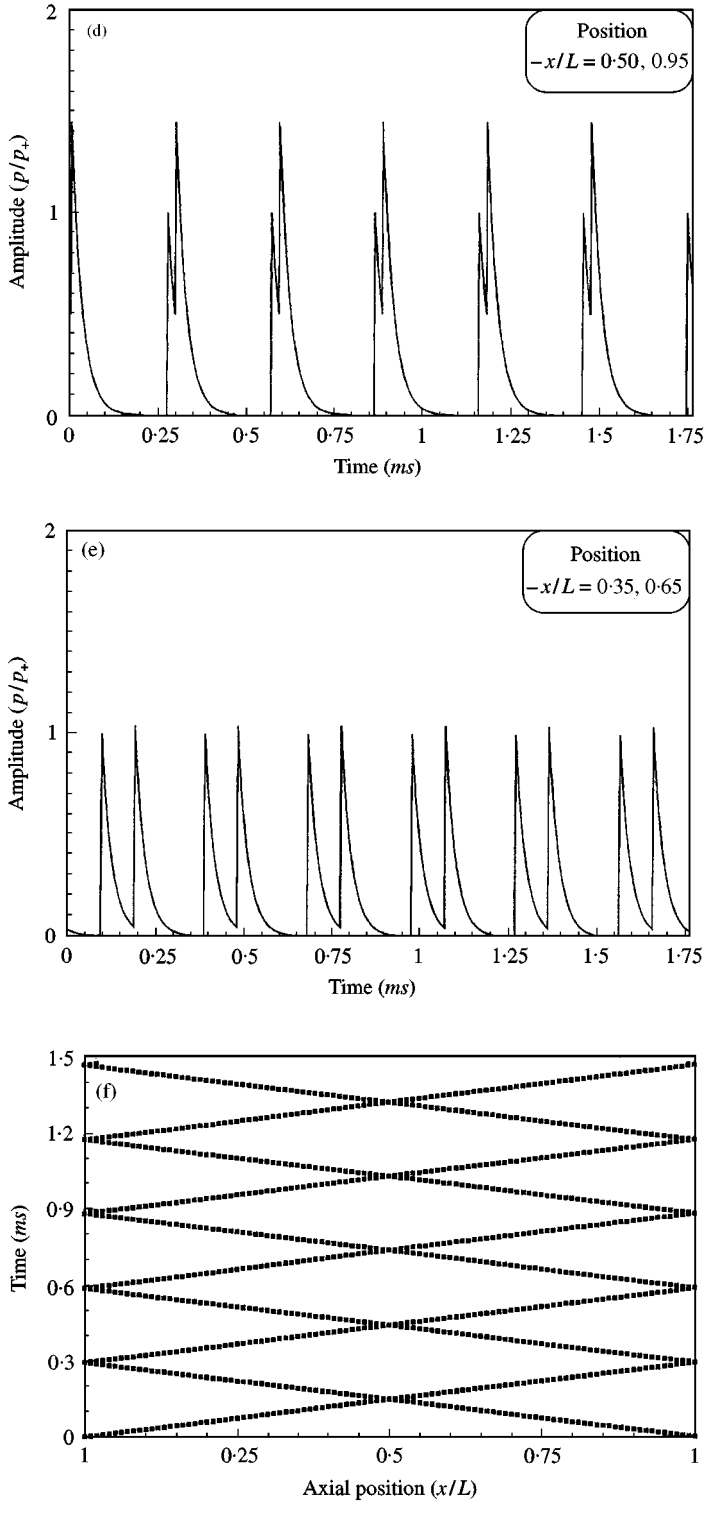

Figure 5. (d) Time variation of pressure at $x/L = 0{\cdot}05$; $0{\cdot}95$; (e) time variation of pressure at $x/L = 0{\cdot}35$, $0{\cdot}65$; (f) phase diagram.

respectively. Since waves measured in the chamber are steep, the phase variation curve is diamond shape. In order to generate the first mode numerically, waves with wavelength of twice the pipe length are imposed at the two ends of the pipe and have one period phase difference with respect to each other. For the third mode, the wavelength of the imposed waves is $\frac{2}{3}$ of the pipe length and their phase difference is half of their period.

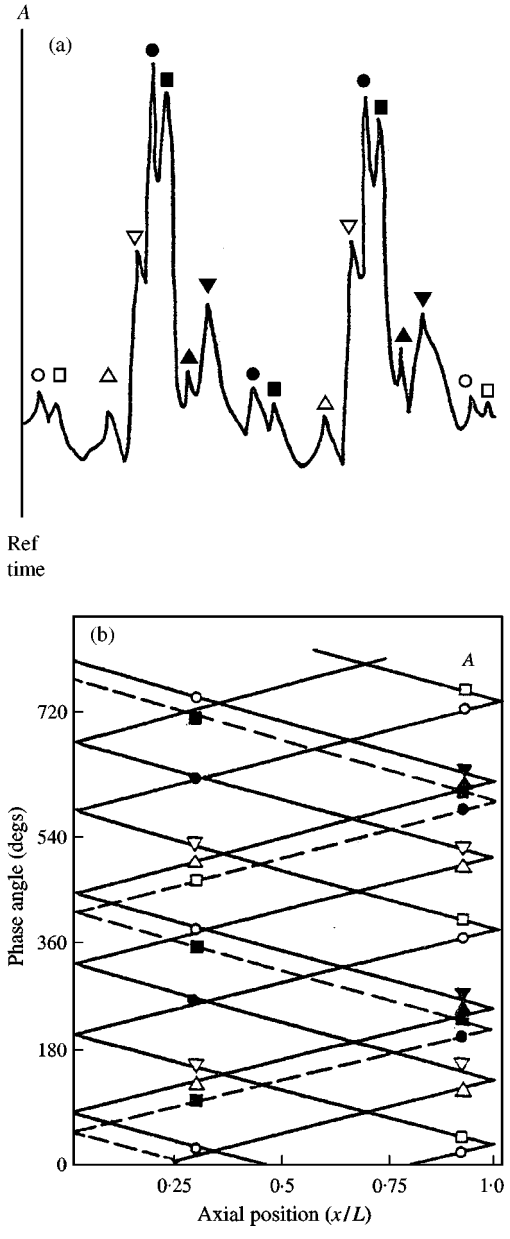

Figure 6. Pressure variation and phase diagrams for coexisting first and third steep longitudinal instabilities [3]: (a) time variation of pressure at $x/L = 0{\cdot}9$; (b) phase diagram.

The solution to acoustic equations with above boundary conditions give the time variation of pressure at point $x/L = 0{\cdot}9$ and phase variation along the pipe, as shown in Figure 7(a) and (b) respectively. The phase curve matches very well with the results of previous work [3]. For the pressure variation at the point $x/L = 0{\cdot}9$, eight consecutive peaks are observed which are repeated continuously. The amplitude of the oscillations do not match very well. However, results of the numerical solution of the acoustic equations can be used for the identification of acoustic modes in a chamber. This method becomes complicated when

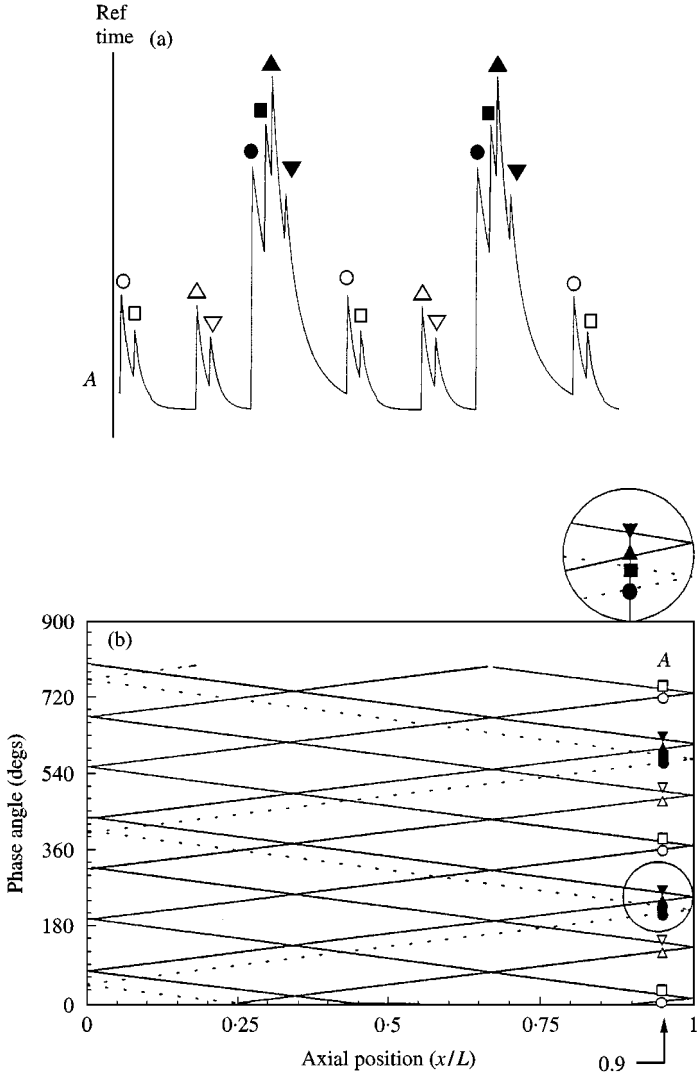

Figure 7. Computed pressure variation and phase diagrams for coexisting first and third steep longitudinal instabilities: (a) time variation of pressure at $x/L = 0{\cdot}9$; (b) phase diagram – – – – first mode; —— third mode.

interaction of higher order modes exists and other complementary methods should be used.

5. CONCLUSION

A single measurement of pressure by a high-response pressure transducer is sufficient to indicate the existence of combustion instability in the rocket engine. Regardless of the diagnostic tools, exact determination of instability modes and their identification of being one of travelling, standing, spinning, and precessing forms, need reconstruction of the waves by numerical means. This work presents a relatively simple tool for recognition and identification of various harmonic and steep waves existing in the combustion chamber. According to the computations and comparisons made, the principle of superposition can be used for all types of non-linear waves observed in combustion chambers as well. Thus, at least in simple situations, if non-linear waves are observed in pressure measurements, this method can be used to identify the non-linear modes.

ACKNOWLEDGMENTS

The authors extend their appreciation to research deputy of Sharif University of Technology for its support.

REFERENCES

1. L. Crocco and D. T. Harrje 1963 *Experimental Method in Combustion Research* (*AGARD*), 30–52. Combustion instability in liquid propellant rocket motors.
2. R. R. Weiss 1996 *Technical Report AFRPL-TR*-66-150. An introduction to combustion instability in liquid propellant rocket engines.
3. D. T. Harrje and F. H. Reardon 1972 *NASA SP*-194. Liquid propellant rocket combustion instability.
4. L. Crocco 1965 *Tenth Symposium* (*International*) *on Combustion*, 1101–1128. Theoretical studies on liquid propellant rocket instability.
5. F. E. C. Culick 1989 *AGARD Conference Proceedings No.* 4501-70. Combustion instability in liquid-fueled propulsion systems — an overview.
6. F. R. Reardon, L. Crocco and D. T. Harrje 1964 *Journal of the American Institute of Aeronautics and Astronautics* **2**, 1631–1641. Velocity effects in transverse mode liquid propellant rocket combustion instability.
7. L. Crocco, J. Grey and D. T. Harrje 1960 *Journal of the American Rocket Society* 159–168. Theory of liquid propellant rocket combustion instability and its experimental verification.
8. H. Y. Ken, A. Trouve and J. W. Daily 1991 *Journal of Fluid Mechanic* **232**, 47–72. Low frequency pressure oscillations in a model ramjet combustor.
9. P. Akbari 1998 Experimental investigation of combustion instability in a model ramjet. *M.Sc. thesis*, Sharif University of Technology, Iran.
10. R. B. Lawhead 1963 *Eighth Symposium* (*International*) *on Combustion*, 1140–1151. Photographic studies of combustion processes in liquid propellant rockets.

11. R. S. Levine 1965 *Tenth Symposium* (*International*) *on Combustion*, 1083–1099. Experimental status of high frequency liquid rocket combustion instability.
12. B. van Leer 1982 *Lecture Notes in Physics* **170**, 507–512. Flux vector splitting for the Euler equations.
13. C. Hirsch 1990 *Numerical Computation of Internal and External Flows*, Vol. 2. New York: Wiley.
14. H. C. Yee 1989 *NASA TM*-101088. A class of high resolution explicit and implicit shock capturing methods.
15. L. D. Landau and E. M. Lifshitz 1987 *Fluid Mechanics*, Vol. 6. Oxford: Pergamon Press, Course of Theoretical Physics, Second edition.
16. M. Barrere *et al.*, 1959 *Rocket Propulsion*. New York: Van Nostrand Company.

APPENDIX: NOMENCLATURE

a velocity of sound, m/s
c Courant number
E total internal energy, kJ/kg
F components of flux vector
$\mathbf{F}$ flux vector
$\tilde{\mathbf{F}}$ numerical flux vector
H total enthalpy, kJ/kg
H enthalpy, kJ/kg
i cell index
L tube length, m
M Mach number, u/a
p pressure, Pa
S cell face area, m^2
T temperature, K
t time, s
U vector of conservative variables
$\tilde{\mathrm{U}}$ vector of primitive variables
u velocity, m/s
v volume, m^3
x axial position, m

GREEK LETTERS

γ specific heat ratio
Δ difference
θ parameter in equations (12), (13)
κ parameter in equations (12), (13)
λ wavelength, m
ρ density, kg/m^3
τ wave period, s
ϕ flux limiter vector

SUBSCRIPT AND SUPERSCRIPT

L	left side
0	reference values
R	right side
$+$	right-travelling wave
$-$	left-travelling wave
*	amplitude of pressure oscillation